A Reaction-Diffusion Model to Study RNA Motion by Quantitative Fluorescence Recovery after Photobleaching

José Braga,* James G. McNally,† and Maria Carmo-Fonseca*
*Instituto de Medicina Molecular, Faculdade de Medicina, Universidade de Lisboa, Lisbon, Portugal; and †Laboratory of Receptor Biology and Gene Expression, National Cancer Institute, National Institutes of Health, Bethesda, Maryland

ABSTRACT Fluorescence recovery after photobleaching (FRAP) is a powerful technique to study molecular dynamics inside living cells. During the past years, several laboratories have used FRAP to image the motion of RNA-protein and other macromolecular complexes in the nucleus and cytoplasm. In the case of mRNAs, there is growing evidence indicating that these molecules assemble into large ribonucleoprotein complexes that diffuse throughout the nucleus by Brownian motion. However, estimates of the corresponding diffusion rate yielded values that differ by up to one order of magnitude. In vivo labeling of RNA relies on indirect tagging with a fluorescent probe, and here we show how the binding affinity of the probe to the target RNA influences the effective diffusion estimates of the resulting complex. We extend current reaction-diffusion models for FRAP by allowing for diffusion of the bound complex. This more general model can be used to fit any fluorescence recovery curve involving two interacting mobile species in the cell (a fluorescent probe and its target substrate). The results show that interpreting FRAP data in light of the new model reconciles the discrepant mRNA diffusion-rate values previously reported.

INTRODUCTION

Eukaryotic cells contain a myriad of RNA species that are implicated in virtually all aspects of gene expression (for a recent review, see Mendes Soares and Valcarcel (1)). Inside the living cell, RNA molecules move between subcellular compartments and assemble into distinct macromolecular complexes that are highly dynamic over time and space. A variety of time-lapse microscopy techniques are currently available to track these movements using fluorescent tags that bind to the RNA (2).

In particular, fluorescence recovery after photobleaching (FRAP) is widely used as a tool to study molecular dynamics in vivo (3–6). FRAP is based on the local perturbation of the fluorescence steady state by inducing irreversible photobleaching with an intense light source, usually a laser. Then, due to the motion of unbleached molecules from regions not affected by bleaching, fluorescence relaxes to a new steady state. The rate by which this relaxation occurs is related to the overall mobility of the molecule: a higher mobility implies a faster recovery of fluorescence inside the bleached region. By bleaching a specific cellular region, FRAP experiments can be used to assess whether a fluorescently tagged molecule is either in constant exchange between two different pools or stably immobilized in a compartment (7–11). For mobile species, a simple step in extracting quantitative information from FRAP experiments is to calculate the half-time of recovery (12). Another approach is to fit recoveries to one exponential (13,14) or a sum of exponentials (15). However, care must be taken, as diffusion-like recoveries are apparently properly fitted with two exponentials, but this type of fitting gives incorrect information about the underlying process. Recent theoretical work (16) shows that recovery curves that seem to contain two recovery phases cannot necessarily be separated into two distinct processes occurring at different timescales (17). Estimating quantitative parameters, such as diffusion coefficient, immobile fractions, or binding rates from FRAP experiments, is a complex task for which several methods have been proposed (16,18–22). Of these, the most widely used in cell biology was the one developed by Axelrod for measuring diffusion rates (18,23–25).

Currently, a large body of evidence indicates that eukaryotic mRNAs form large ribonucleoprotein particles (RNPs) that are transported from the sites of transcription to the nuclear pores by random Brownian motion (18,26–31). However, estimates of the corresponding diffusion rate yielded values ranging from 0.03–0.04 $\mu m^2\ s^{-1}$ (29–31) to 0.6 $\mu m^2\ s^{-1}$ (18,27,32). In most of these experiments, the mRNAs were tagged with a small fluorescent probe, either an oligonucleotide or an RNA-binding protein. Since these probes are themselves mobile in the cell and they fluoresce regardless of whether or not they bind to the RNA, it was proposed that nonbound probe molecules may contribute to the fluorescence recovery after photobleaching and consequently lead to an overestimation of the mRNA diffusion rate (29). Here, we tested this possibility, and we show numerically how the binding affinity of a fluorescent probe to its substrate affects the measurement of the effective diffusion coefficient of the resulting complex. We also show that binding information can be obtained provided that the diffusion coefficients of the two species are known.

Submitted September 11, 2006, and accepted for publication January 5, 2007.

Address reprint requests to José Braga, Institute of Molecular Medicine, Faculty of Medicine, Av. Prof. Egas Moniz, 1649-028 Lisbon, Portugal. Tel.: 351-21-7999411; Fax: 351-21-7999412; E-mail: josebraga@fm.ul.pt.

0006-3495/07/04/2694/10 $2.00

doi: 10.1529/biophysj.106.096693

MATERIALS AND METHODS

Cell culture and transfection

HeLa cells were cultured as monolayers in modified Eagle's medium (MEM) supplemented with 10% fetal calf serum (Gibco-BRL, Paisley, Scotland). Cells were plated and observed in glass-bottom chambers (MatTek, Ashland, MA). For imaging, the medium was changed to D-MEM/F-12 without phenol red, supplemented with 15 mM HEPES buffer (Gibco). Subconfluent cells were transiently transfected using FuGENE6 reagent (Roche Biochemicals, Indianapolis, IN).

Confocal microscopy and FRAP image analysis

Live-cell microscopy was performed on a confocal microscope (Axiovert 100 M with LSM 510 scanning module, Zeiss, Jena, Germany) using the PlanApochromat 63×/1.4 objective. EGFP fluorescence was detected using the 488-nm line of an Ar laser (25 mW nominal output) and a LP 505 filter. Cells were maintained at 37°C on a heating frame (LaCon GbR, Staig, Germany), in conjunction with an objective heater (PeCon GmbH, Zurich, Switzerland).

FRAP experiments were performed as previously described (18). Bleaching beam parameters were obtained from immobilized molecules, as described in Braga et al. (22). During scanning, the transmission of the acoustic optical tunable filter was set to 1% of laser power. Bleaching was performed at maximum transmission of the laser. The bleaching time was 110 ms for a circular bleach region of interest (ROI) of 0.71-μm radius. The bleached ROI was scanned, on average, 39 ms after the end of bleaching, and images were acquired with intervals of 78 ms.

RESULTS

Derivation of a reaction-diffusion model with two interacting mobile molecules

To estimate the mobility rate of a complex formed by two interacting molecular species in vivo, we assumed a binding reaction of the form

$$F + S \leftrightarrows C, \tag{1}$$

where F and S refer to the nonbound individual species and C is the complex formed by the reaction. The F species is fluorescently tagged, whereas S represents the nonfluorescent target substrate; C becomes indirectly tagged when the binding reaction occurs. We assumed that the substrate (S) is homogenously distributed during the course of the experiment and does not contribute to the measured fluorescence. The system is further assumed to be at equilibrium at all times and we denote the equilibrium concentrations of each species by the subscript ''eq''. Before bleaching, all species are considered to be homogenously distributed around the bleached region. In the case of PABPN1 this is an approximation, because the protein distributes throughout the nucleoplasm, with higher accumulation at nuclear speckles (Fig. 1 *A*).

The duration of each FRAP experiment (~8 s) is much shorter than the time required to synthesize new fluorescent proteins (it takes 30–60 s to synthesize an average-sized eukaryotic protein). Consequently, the total amount of each species (including visible plus bleached molecules) is constant during the experiment. We assumed that bleached and unbleached molecules have exactly the same kinetic behavior and that bleaching does not affect chemical equilibrium, as it only disturbs the spatial distribution of the visible part of the system. Finally, we assumed that bleaching is a first-order linear process taking a finite amount of time. As previously shown, the axial extension of the bleached volume, even for a high NA objective, is larger than the cell thickness (22). This is consistent with a recent study showing that, with high illumination intensities, the dimensions of the bleaching beam can be larger than the theoretical expectations (33,34). Thus, as in other studies (16,35), we will consider that recovery of fluorescence is essentially two-dimensional. The limitations of this approximation are explored elsewhere (19)

The resulting reaction-diffusion system is mathematically translated as

$$\begin{aligned}\frac{\partial F}{\partial t} &= D_F\nabla^2 F - k_{on}S_{eq}F + k_{off}C - \beta I(\vec{r},t)F\\ \frac{\partial C}{\partial t} &= D_C\nabla^2 C + k_{on}S_{eq}F - k_{off}C - \beta I(\vec{r},t)C,\end{aligned} \tag{2}$$

where F is the concentration of the nonbound fluorescent molecules, D_F is their diffusion coefficient, S is the concentration of the target substrate, C is the concentration of the fluorescent complex, and D_C is its diffusion coefficient. β, the bleach rate, is a constant proportional to the bleaching susceptibility of the fluorophore, and k_{on} and k_{off} are the on and off rates of the chemical reaction. I(r,t) is the bleaching laser intensity, which will be modeled as a Gaussian laser beam of the form (22)

$$I(r,t) = \begin{cases} I_0\exp\left(-2\dfrac{r^2}{w^2}\right) & t < T_B \\ 0 & t > T_B \end{cases}, \tag{3}$$

where I_0 is the maximum intensity of the laser, w is the e^{-2} beam width, and T_B is the duration of bleaching.

The compartment under study, the nucleus, is considered to have a finite size with circular geometry (with radius $R_{nucleus}$). Bleaching is performed at the center of the circle. The boundary and initial conditions are then

$$\begin{aligned}&F(\vec{r},0) = F_{eq};\ C(\vec{r},0) = C_{eq}\\ &\frac{\partial}{\partial r}F(R_{nucleus},t) = 0;\ \frac{\partial}{\partial r}C(R_{nucleus},t) = 0.\end{aligned} \tag{4}$$

The dissociation constant of a chemical reaction (K_D) is defined as

$$K_D \equiv \frac{k_{off}}{k_{on}} \tag{5}$$

and is related to the equilibrium concentrations of the reagents by

$$K_D \equiv \frac{F_{eq}S_{eq}}{C_{eq}}. \tag{6}$$

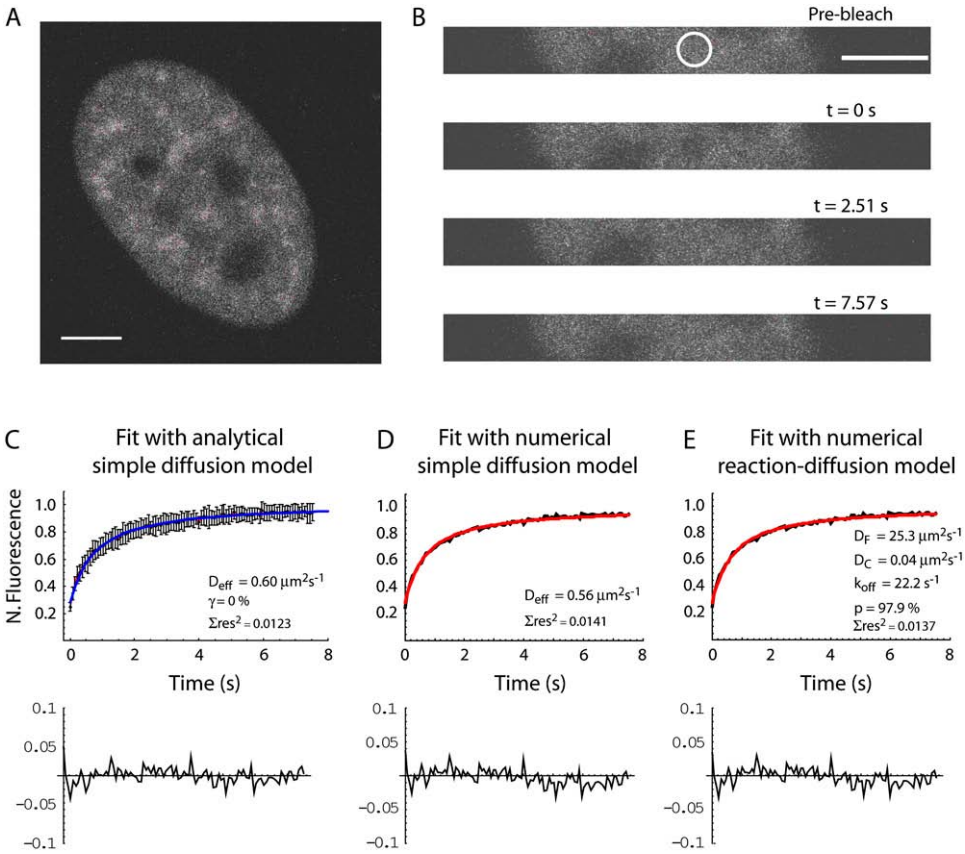

FIGURE 1 Fitting FRAP curves with simple diffusion and reaction-diffusion models. (*A*) Cells expressing GFP-PABPN1 were imaged at 37°C. PABPN1 has a typical nucleoplasmic distribution with increased concentration in nuclear speckles. (*B*) For faster imaging during FRAP experiments, the number of lines is increased. Represented are images taken before bleaching, the first image after bleaching ($t = 0$ s), at $t = 2.51$ s, and at $t = 7.57$ s. Bleaching was performed in a circular region of 0.71-μm radius in the nucleoplasm (outside the speckles). The total nucleoplasmic radius at an equatorial image ranges between 5 and 12 μm. (*C*) The experimental data correspond to the average of three independent experiments with 10 cells analyzed per experiment (*black lines*). Error bars represent standard deviations of fluorescence values. According to the simple diffusion models (*C* and *D*), nonbound GFP-PABPN1 molecules and GFP-PABPN1 molecules bound to poly(A)-RNA are considered two independent populations; as most GFP-PABPN1 molecules are associated with RNA in the nucleus (see Discussion), the model assumed a single-component diffusion. In *C*, an analytical model was used (22), yielding estimates of the effective diffusion coefficient (D_{eff}) and immobile fraction (γ). In *D*, we used a numerical approach (see Results), which optimizes only for a single parameter, D_{eff}. According to the reaction-diffusion model (*E*), the bound and nonbound pools of GFP-PABPN1 molecules are in constant exchange. The diffusion coefficients of the free and bound species (D_{F} and D_{C}, respectively) are fixed parameters (see Results for justification of values) and the fitting procedure yields the off rate of the reaction (k_{off}) and the fraction of molecules bound to the mRNA (p). All fits (*red lines*) follow closely the experimental data and give similar minima for Σres^2. Below each fit are plots of the residuals showing that experimental values differ from the estimates by <10% in all cases.

A lower value of the dissociation constant corresponds to a higher affinity of the nonbound species for its substrate.

For some of our analysis, it is useful to eliminate k^*_{on} and S_{eq} from Eq. 2. For this, we denote the percentage of fluorescent molecules bound to the substrate before bleaching by the letter p. The equilibrium concentration of nonbound substrate species is thus given by

$$S_{\text{eq}} = K_{\text{D}} \frac{p}{1-p}, \tag{7}$$

and the pseudo-on rate ($k^*_{\text{on}} = k_{\text{on}} S_{\text{eq}}$) by

$$k^*_{\text{on}} = k_{\text{off}} \frac{p}{1-p}. \tag{8}$$

Since the system is at equilibrium and the substrate molecules (S) are not affected by bleaching, the concentration of S is constant throughout the experiment, making Eq. 2 linear.

In previous works, researchers quantitatively analyzed FRAP experiments by investigating the contribution of binding interactions to immobile substrates ($D_{\text{C}} = 0\ \mu\text{m}^2\ \text{s}^{-1}$) (16,19,36,37). In this work, we aim to extend analysis of previous studies by considering the case of diffusing substrates ($D_{\text{C}} > 0\ \mu\text{m}^2\ \text{s}^{-1}$). In this case, the expected FRAP behaviors over a broad range of reaction parameters will be analyzed in detail (see below). Equation 2 becomes

$$\begin{aligned} \frac{\partial F}{\partial t} &= D_{\text{F}} \nabla^2 F - k_{\text{off}} \frac{p}{1-p} F + k_{\text{off}} C - \beta I(\vec{r}, t) F \\ \frac{\partial C}{\partial t} &= D_{\text{C}} \nabla^2 C + k_{\text{off}} \frac{p}{1-p} F - k_{\text{off}} C - \beta I(\vec{r}, t) C. \end{aligned} \tag{9}$$

To the best of our knowledge, no general analytical solutions are available to solve Eq. 9 with the boundary conditions given by Eq. 4. Thus, simulated FRAP curves are generated from the numerical solution of Eq. 9. The solutions were computed using the function NDSolve of Mathematica 4.0 (Wolfram Research, Champaign, IL). We compared simulated FRAP curves obtained for different radii of the nucleus (last line of Eq. 4.) and we found that if the size of the cellular compartment being analyzed is at least fourfold larger than the bleach spot, the differences are not significant. These computer-generated FRAP recovery curves were obtained using the actual experimental values for fluorophore

and bleaching beam parameters. Assuming a Gaussian bleach, we determined the beam width in the radial direction, the size of the bleach ROI, and the bleach efficiency (K) according to Braga et al. (22). We also took into account the duration of bleach phase and acquisition parameters (such as the time between images, the starting time of the imaging phase, and the total duration of the FRAP experiment).

Considering that GFP (27 kDa) diffuses in cells at 33 $\mu m^2\ s^{-1}$ (22), unbound GFP-PABPN1 molecules (~60 kDa) are expected to diffuse at ~25.3 $\mu m^2\ s^{-1}$ (16).

Parameters that were specifically optimized for the simulations were the off-rate constant and the fraction of the tag bound to the substrate molecules (p). The optimization space was comprehensively explored by computing FRAP curves for many points in this space. The numerical solutions obtained were compared with the experimental data, and we selected the solution that minimized the sum of the squares of the residuals (Σres^2).

Fitting of experimental curves with a numerical simple diffusion model was performed by setting the fraction of bound molecules to zero. The parameter to be optimized was the diffusion coefficient of the free species.

Effective diffusion regimes for the reaction-diffusion model

For the special case when $D_C = 0$, several studies (16,38) have demonstrated that the FRAP equations can be simplified under certain conditions. One simplification arises when the binding reaction is fast compared to the diffusion time. In this case, the FRAP equations can be reduced to a simple diffusion equation. The effective diffusion constant (D_{eff}), however, is smaller than the free diffusion constant (D_F) and given by $D_{eff} = D_F(1 - p)$. This effective diffusion behavior has been observed for several different nuclear proteins, and so we investigated what the analog of this behavior would be for the case where D_C is nonzero.

After bleaching, Eq. 2 becomes

$$\frac{\partial F}{\partial t} = D_F\nabla^2 F - k^*_{on}F + k_{off}C$$
$$\frac{\partial C}{\partial t} = D_C\nabla^2 C + k^*_{on}F - k_{off}C. \quad (10)$$

Adding these two equations yields

$$\frac{\partial F}{\partial t} + \frac{\partial C}{\partial t} = D_F\nabla^2 F + D_C\nabla^2 C. \quad (11)$$

When $1/k^*_{on}$ is very fast relative to the time to diffuse at rate D_F across the bleach spot, there is a local chemical equilibrium that arises throughout the FRAP recovery. In a local instantaneous chemical equilibrium, we have $k^*_{on}F \approx k_{off}C$. As a result,

$$C \approx (k^*_{on}/k_{off})F = \alpha F. \quad (12)$$

Substituting this into Eq. 9 yields

$$\frac{\partial F}{\partial t} + \alpha\frac{\partial F}{\partial t} = D_F\nabla^2 F + \alpha D_C\nabla^2 F. \quad (13)$$

Collecting terms, this produces an effective diffusion equation for this local equilibrium condition:

$$\frac{\partial F}{\partial t} = \frac{D_F + \alpha D_C}{1 + \alpha}\nabla^2 F, \quad (14)$$

where the effective diffusion coefficient is seen to be

$$D_{eff} = (D_F + \alpha D_C)/(1 + \alpha). \quad (15)$$

Thus, in the case of fast reactions, the effective diffusion coefficient depends on the ratio k^*_{on}/k_{off}. Using the fact that $\alpha = p/(1 - p)$, Eq. 15 can be written as

$$D_{eff} = (1 - p)D_F + pD_C, \quad (16)$$

indicating that the effective diffusion coefficient is the weighted average of the unbound fraction diffusing at D_F and the bound fraction diffusing at D_C. Note that this is a generalized effective diffusion coefficient and reduces to the ''classical'' one when $D_C = 0$. Equation 16 shows that when effective diffusion is occurring, D_C can be directly measured only if the vast majority of molecules are bound. In such a case, $p = 1$, and so $D_{eff} = D_C$.

Fitting FRAP experiments with simple diffusion and reaction-diffusion models

We previously reported the use of GFP-tagged PABPN1 to estimate the diffusion coefficient of poly(A)-RNA in the nucleus (18). Fitting the experimental FRAP recovery curves with a simple diffusion model according to Axelrod's method (18,25,39) resulted in an estimated diffusion coefficient of 0.6 $\mu m^2\ s^{-1}$ and no immobile fraction (18). Similar values were obtained when the fitting was performed according to the method described by Braga et al. (22), which is also based on a simple diffusion model but takes into account diffusion of fast-moving molecules during the bleach period (Fig. 1 *C*). The sum of the square of the residuals (Σres^2) was found to be 0.0123, indicating that the fitting curve follows accurately the average values of the FRAP curve. Residual differences between the model and experimental data were at most 8%. Application of a numerical method considering simple diffusion yielded similar results ($D = 0.56\ \mu m^2\ s^{-1}$ (Fig. 1 *D*)), with a slightly higher value of Σres^2 (0.0141), and also low values of residuals (7%). Note that the only parameter being optimized in all of these cases is the diffusion coefficient.

Consistent with published fits (18,32), the data in Fig. 1, *C* and *D*, could mean that polyA RNA diffuses at a rate given by $D \approx 0.6\ \mu m^2\ s^{-1}$. However, in vitro assays reveal that binding of PABPN1 to poly(A)-RNA is a reversible process (40). Such binding interactions are also likely to occur in vivo, and therefore, rather than a pure diffusion model, a

reaction-diffusion model is necessary to accurately describe the FRAP recovery of GFP-PABPN1.

To address this, we developed the reaction-diffusion model described above. In the model, GFP-PABPN1 is presumed to bind reversibly to poly(A)-RNA, and the two species, GFP-PABPN1 (the fluorescent, nonbound molecular form, *F*) and poly(A)-RNA (the substrate, *S*), are assumed to diffuse, though at different rates. The system is considered to be at a steady state by the time the FRAP experiment is performed, and all molecular species are homogenously distributed throughout most of the nuclear volume.

As a first test, we asked whether this reaction-diffusion model could explain the FRAP data if the diffusion constant for poly(A)-RNA was much smaller ($D_C = 0.04\ \mu m^2\ s^{-1}$), namely, equal to the estimates obtained by other (non-FRAP) techniques (29,31). We also fixed the diffusion constant of the unbound GFP-PABPN1 at $D_F = 25.3\ \mu m^2\ s^{-1}$, based on the measured diffusion constant of free GFP and the increased size of PABPN1. Then, the FRAP data were fit with two free parameters, the bound fraction (p) and the off rate (k_{off}). Fitting was performed by choosing the numerically simulated recovery curve that minimized the sum of squares of the residuals (Σres^2) to the experimental curve (see Fig. 1 *E*). The minimum for Σres^2 (0.0137) occurred for $k_{off} = 22.2\ s^{-1}$ and $p = 97.9\%$ (or $k^*_{on} = 1.04\times10^3\ s^{-1}$), with residuals similar to the previous fit (Fig. 1 *B*). Thus, a reaction-diffusion model with a much slower diffusion constant for poly(A)-RNA can also account for the FRAP recovery.

To determine the sensitivity of the preceding fit to k_{off} and p, we tested the behavior of Σres^2 in the neighborhood of the minimum (Fig. 2 *A*). We found that this function varies rapidly in the direction of p, but varies very smoothly in the direction of k_{off}. For example, values of $\Sigma res^2 < 0.01385$ (a value only slightly higher than the absolute minimum) are tightly concentrated around $p = 97.9\%$ but the corresponding k_{off} values spread widely from 14 s^{-1} to 30 s^{-1}. In fact, Fig. 2 suggests that any k_{off} value $>\sim10\ s^{-1}$ will yield a good fit. Thus when the diffusion constants D_F and D_C are fixed, the FRAP data will yield a good estimate for the bound fraction p, but not for the off rate k_{off}.

Next, we tested whether different values of the diffusion coefficients of the free and bound species could also account for the experimental data (Fig. 2, *B–D*). We found that in these conditions, equally good fits to the experimental data are obtained and the minimum of Σres^2 is 0.0137 in all cases.

The results in Fig. 2 indicate that the reaction-diffusion model provides a good estimate of the bound fraction p, but

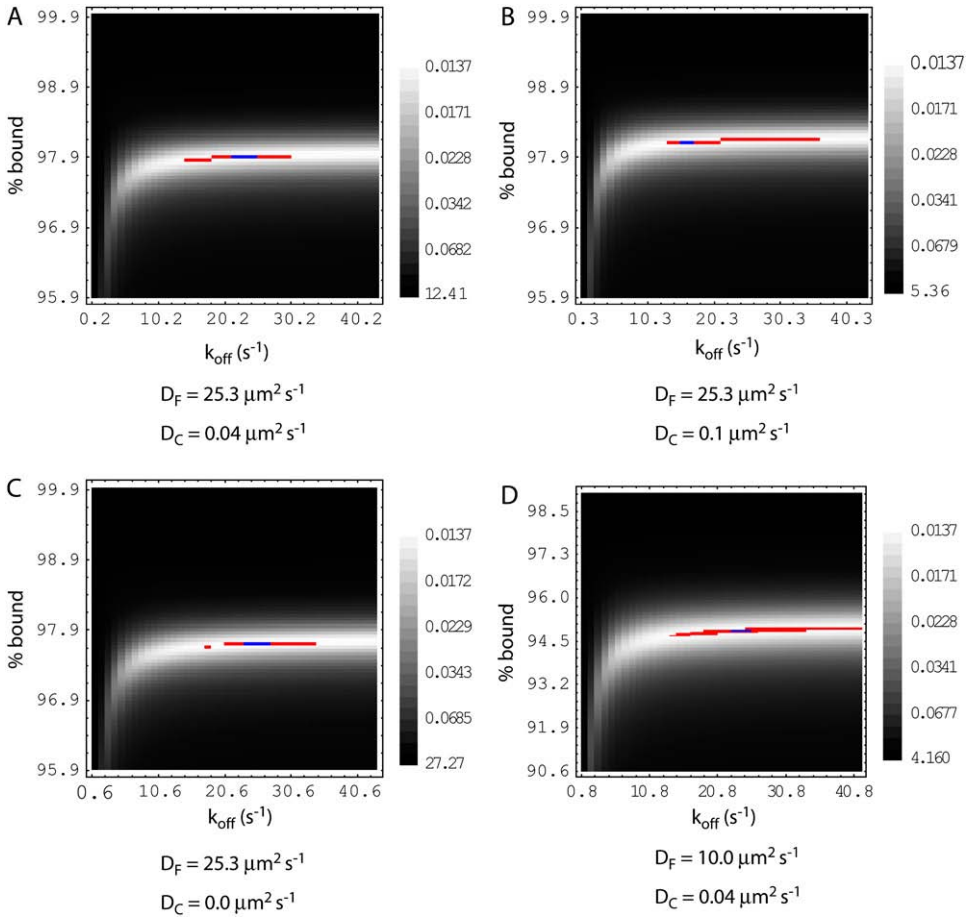

FIGURE 2 Behavior of Σres^2 in the neighborhood of the minimum. The density graphs plot the values of Σres^2 as a function of the off rate of the reaction (k_{off}) and the fraction of molecules bound to the mRNA. The red line depicts points for which Σres^2 is <1% higher than the value of the absolute minimum, and the blue line depicts points that are < 0.1% higher than the minimum. In all graphs, Σres^2 varies steeply with p, whereas for k_{off} several values give results close to the absolute minimum. Thus, these data indicate that the optimal values of k_{off} are probably not bounded. No other local minima were found. (*A*) Using the expected values for the diffusion coefficients (as discussed in Results), $D_F = 25.3\ \mu m^2\ s^{-1}$ and $D_C = 0.04\ \mu m^2\ s^{-1}$. (*B*) Increasing the mobility of the complexes 2.5 times, $D_C = 0.1\ \mu m^2\ s^{-1}$. (*C*) Decreasing the mobility of the complexes, $D_C = 0.0\ \mu m^2\ s^{-1}$. (*D*) Decreasing the mobility of the free molecules, $D_F = 10.0\ \mu m^2\ s^{-1}$. Though substantial variations were made in the diffusion components, fitting consistently found values around 20 s^{-1} for k_{off} and >94% for p. In all the graphs, the minimum value of Σres^2 is the same (0.0137), i.e., it is independent of the values chosen for D_F and D_C.

not of k_{off}, D_F, or D_C. The results in Fig. 1 show that good fits to the FRAP data can also be obtained with a simple diffusion model that does not incorporate a binding interaction at all, even though such interactions are likely to be occurring. This combination of circumstances has been observed before in the case of immobile binding sites (16,19), and is characteristic of a simplified form of the reaction-diffusion model known as effective diffusion. Thus, we wondered whether a comparable scenario could explain our observations with a model incorporating mobile binding sites.

To test this, we derived the effective diffusion simplification for the case of mobile binding sites (see previous section). We found that FRAP recoveries could also mimic pure diffusion under certain conditions, but with a generalized effective diffusion constant of $D_{eff} = (1 - p)D_F + pD_C$. This result implies that the estimates for D in Fig. 1 could in fact reflect an effective diffusion constant, not pure diffusion of the poly(A)-RNA. If so, then the estimates obtained for D in Fig. 1 should also be consistent with the estimates obtained for p in Fig. 2 and the preceding equation for D_{eff}. Using $D_{eff} = 0.56\,\mu m^2\,s^{-1}$ (as estimated by the numerical diffusion fit (Fig. 1 *D*)) and the corresponding D_F and D_C for each graph in Fig. 2, we obtain, using the effective diffusion equation above, $p = 97.9\%$ (Fig. 2 *A*), $p = 98.2\%$ (Fig. 2 *B*), $p = 97.8\%$ (Fig. 2 *C*), and $p = 94.8\%$ (Fig. 2 *D*). Thus, the predicted values for p correspond exactly to the estimates for p obtained from the full reaction-diffusion model, and the effective diffusion equation above also explains why the only parameter well determined by the fit is p. Together, these results strongly argue that effective diffusion is a reasonable explanation for the FRAP recovery of GFP-PABPN1.

Naturally, for the fit to be possible, D_C should be lower than the effective diffusion coefficient measured with a simple diffusion model. However, 2.5-fold changes in D_C or D_F do not result in large changes in the estimates of p (Fig. 2). The values found by the optimization procedure in these different situations are in agreement and demonstrate that a large percentage of PABPN1 is bound to the mRNA (>94%) and that k_{off} is $>\sim 10\ s^{-1}$. The reaction is too transient for k_{off} to be accurately measured by photobleaching techniques. This situation was also found in previous studies (19). In fact, Eq. 16 shows that in an effective diffusion regime, only p significantly contributes to the effective mobility measurements.

In conclusion, our results show that FRAP recovery curves obtained with GFP-PABPN1 can be equally fitted by two distinct models. Assuming that the recovery after photobleaching reflects exclusively the dynamics of GFP-PABPN1 molecules bound to poly(A)-RNA, the estimated diffusion coefficient of the complex is 0.6 $\mu m^2\ s^{-1}$, as previously reported (18). However, introducing the new model that takes into account that binding of GFP-PABPN1 to poly(A)-RNA is reversible in the cell, the experimental data becomes compatible with a diffusion coefficient of the complex an order of magnitude slower ($\sim$0.04 $\mu m^2\ s^{-1}$).

Influence of binding affinity on estimates of diffusion coefficient

The preceding analysis suggests that for the case of PABPN1 the full reaction diffusion equations for FRAP can simplify to effective diffusion behavior. To investigate more generally when this reduction to the simpler effective diffusion model may occur, we varied k^*_{on} and k_{off} over a large range while holding D_F and D_C constant, and compared a diffusion model solution to the full model solution by computing the Σres^2 between the two curves.

We found reasonably good agreement for most values of k^*_{on} and k_{off} (Fig. 3 *A*), with only a small subset of these values giving rise to clear differences between the FRAP curves (Fig. 3 *A*, *red-outlined area*). To determine whether these regions of good agreement could be explained by the effective diffusion theory, we plotted the difference between the predicted D_{eff} (Eq. 16) and the D_{est} obtained from the diffusion model fit. This difference was negligible over a large region of the space (Fig. 3 *B*, area outside the *blue curve*), indicating that Eq. 16 for effective diffusion could account for all of the FRAP curves in this large region.

We further analyzed this region of agreement with the effective diffusion theory by considering two limiting cases. First, when virtually all molecules are tightly bound to the mobile substrate, then $p \approx 1$ (and k^*_{on}/k_{off} is large) and, by Eq. 16, $D_{est} = D_{eff} \approx D_C$. This situation arises in the area above the blue line in Fig. 3 *C*. Second, when virtually no molecules are bound to the mobile substrate, then $p \approx 0$ (k^*_{on}/k_{off} is small) and, by Eq. 16, $D_{est} = D_{eff} \approx D_F$. This situation arises in the area beneath the green line in Fig. 3 *C*. The latter region is the analog of the pure diffusion domain in which binding interactions are negligible, as previously identified for the case of an immobile substrate (16).

Note that although the region between the blue and red contour lines in Fig. 3 *C* was well fit by a diffusion model, D_{est} did not agree with D_{eff}, as predicted by Eq. 16. We call this region the pseudoeffective diffusion domain (Fig. 3 *D*). Good fits of the diffusion model in this domain may be fortuitous, or they may reflect another, not yet identified, simplification of the full model equations.

In sum, several regions have been empirically identified by the preceding analysis (Fig. 3 *D*):

1. The pure-diffusion regime, which, as in Sprague et al. (16), occurs when binding is weak. In this case, a diffusion model can be used to fit FRAP data, and diffusion estimates are compatible with Eq. 16 and a negligible bound fraction ($p \approx 0$).
2. The effective diffusion regime, which as in Sprague et al. (16), occurs when k^*_{on} is larger than the characteristic diffusion time (w^2/D_F). In this case, a diffusion model

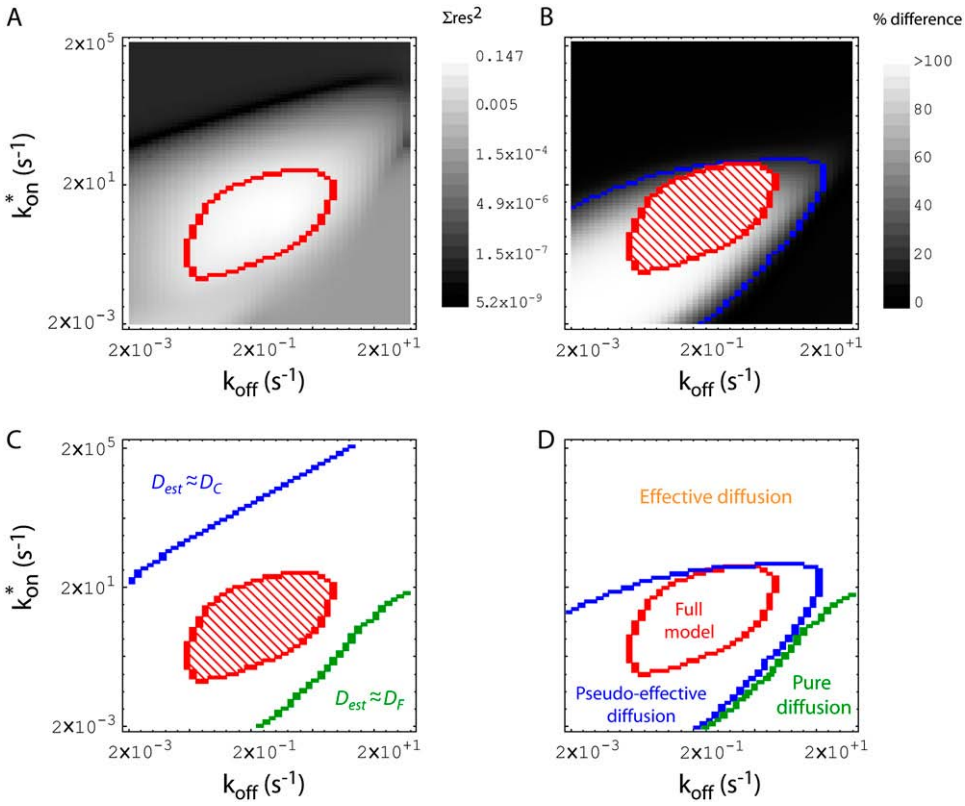

FIGURE 3 Global view of the reaction space. k_{off} was varied between 2×10^{-3} s^{-1} and $6 \times 10^{+1}$ s^{-1} and k^*_{on} between $2 \times 10^{-3}\,s^{-1}$ and $2 \times 10^{+5}\,s^{-1}$, and for each pair of k_{off} and k^*_{on} a simulated FRAP curve was generated. All graphs are log-log plots for k^*_{on} and k_{off}. (*A*) The density graph plots Σres^2 values for each reaction space point. The region delimited by the red line contains points for which $\Sigma res^2 > 0.03$ (a threshold selected to qualitatively discriminate fits that were unsuccessful), indicating that inside this region a diffusion model is not able to properly fit data. (*B*) The density graph plots the difference between the predicted D_{eff} from Eq. 15 and the fitted D_{est}. The blue line contains the region for which a large disagreement (>20%) exists between estimates. Differences drop rapidly to small values outside this region. (*C*) The corresponding estimated diffusion coefficients. The green line shows the boundary of the region for which $D_{est} \approx D_F$ and the blue line the boundary of the region where $D_{est} \approx D_C$ (within a 5% tolerance). (*D*) Based on the findings from *A–C*, several regions can be identified: on the bottom right corner, the pure diffusion region; the full model region, where fits with a simpler diffusion model fail; the effective diffusion region,, in the upper part of the graph, where the diffusion model yields good fits, and simultaneously Eq. 16 is valid, and, finally, the pseudoeffective region, where good fits with a diffusion model are possible but Eq. 16 is not valid.

can also be used to fit FRAP data and diffusion estimates are compatible with Eq. 16 and a measurable bound fraction ($p > 0$).

3. The pseudoeffective diffusion regime, in which a diffusion model can be used to fit FRAP data, but the diffusion estimates are not compatible with Eq. 16.
4. The full model region, which is not fit by a simplified diffusion model.

The preceding analysis demonstrates that a simple diffusion model will often yield a good fit to the full reaction diffusion model. However, D_{est}, as obtained from this simple diffusion fit, will in general not be the same as D_C, the diffusion constant of the mobile substrate, which is actually the quantity of interest. As an example, if the fluorescent probe binds to its substrate with $k_{off} = 22.2\ s^{-1}$ (a residence time of ~50 ms), the effective diffusion coefficient measured will be at least an order of magnitude higher than D_C, even if the bound fraction is as high as 98.5% (Fig. 4 *A*).

To determine how often and by how much D_{est} and D_C may disagree, we computed the ratio D_{est}/D_C as a function of k^*_{on} and k_{off} (Fig. 4 *B*) for points where the simple diffusion model yields a good fit (i.e., outside the red contour line). This plot shows that for very high binding affinities (large k^*_{on}/k_{off}), the value of D_{est} obtained from the simple diffusion fit is a very good estimate of D_C. This occurs only when virtually all of the fluorescent tag is bound to the complex. As the binding affinity of the fluorescent molecule for the substrate decreases, the difference between D_{est} and D_C increases. This is because an increasing fraction of fluorescent molecules become unbound, and instead freely diffuse, confounding the direct estimate of D_C. In the extreme, virtually no fluorescent molecules are bound to the substrate, leading to $D_{est} = D_F$, and thus $D_{est}/D_C = D_F/D_C = 25.3/0.04 \approx 625$, which is the limiting case for the overestimate of D_C with the values of D_F and D_C used here (Fig. 4 *B*, *green contour line* for pure diffusion regime).

As seen in Fig. 4 *B*, the amount that D_C is overestimated changes as a function of the ratio k^*_{on}/k_{off}. When $k^*_{on}/k_{off} = 43.5$, a 15-fold overestimate of D_C occurs. This corresponds to the case for PABPN1 binding to RNA, in which the simple diffusion fit yielded $D_{est} = 0.6\ \mu m^2\ s^{-1}$, 15-fold larger than $D_C = 0.04\ \mu m^2\ s^{-1}$ obtained by single-molecule tracking (29). In that study, mRNA diffusion rates were also estimated by FRAP using a different GFP-tagged mRNA binding molecule, namely MS2. The resultant FRAP curves for GFP-MS2 were then fitted with a simple diffusion model, yielding a value of $D_{est} = 0.09\ \mu m^2\ s^{-1}$. Viewed in light of our current analysis, this value may also be an overestimate due to the fact that MS2 may not be permanently bound to RNA. For MS2, $D_{est}/D_C = 2.25$, corresponding to a predicted in vivo $k^*_{on}/k_{off} = 500$. Thus, our reaction-diffusion model predicts that the in vivo affinity of MS2 for RNA

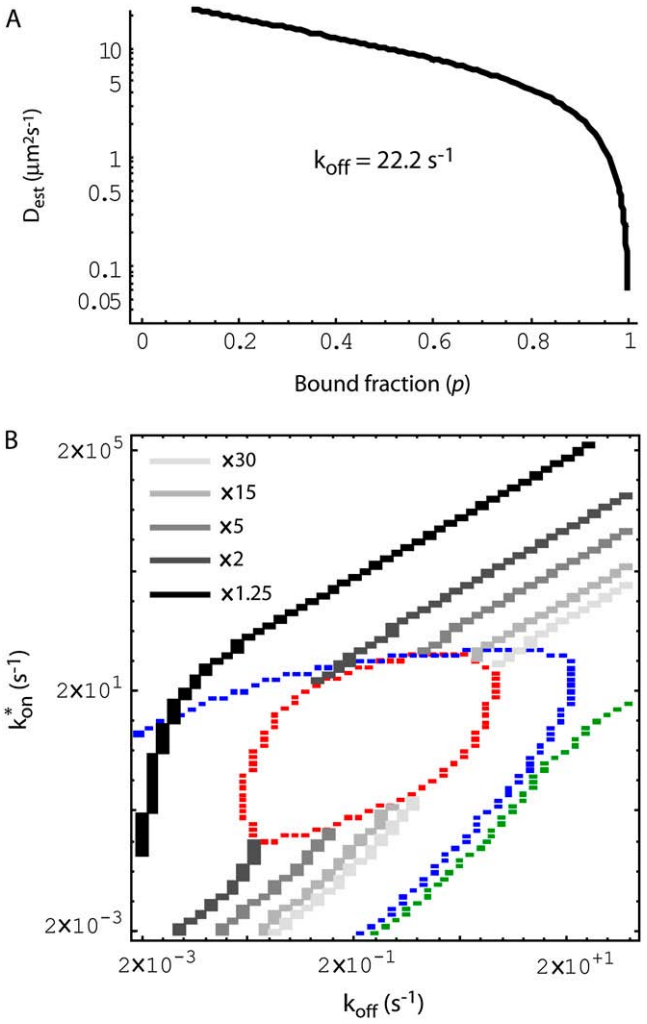

FIGURE 4 Influence of the reaction parameters on the effective diffusion coefficient measured. (*A*) An analytical diffusion model was used to fit simulated FRAP curves with varying p values. Log-linear plot of D_e versus p with constant k_{off} value used (22.2 s^{-1}). In this case, D_{est} is consistently much higher than $D_C = 0.04\ \mu m^2\ s^{-1}$, even if a large proportion (for example, 99.5%) of tagged molecules are bound to the substrate. (*B*) Superimposed over the domain structure of the reaction space (*colored dashed lines*), we represent: the points with the same D_{est}/D_C ratios (30, 15, 5, 2, and 1.25) that are contained within the effective diffusion or pseudoeffective diffusion regimes. As expected for the effective diffusion regime, the lines obtained are straight lines along which the ratio k_{off}/k^*_{on} is constant, located in the positions predicted by Eq. 15.

($k^*_{on}/k_{off} = 500$) is significantly higher than that of PABPN1 for RNA ($k^*_{on}/k_{off} = 43.5$), a result consistent with measurements showing that the in vitro affinity for RNA of MS2 (41) is much higher than the in vitro affinity for RNA of PABPN1 (40).

In sum, our analysis shows that the discrepant values for the mRNA diffusion rate previously reported based on PABPN1 and MS2 can be reconciled if these FRAP results are interpreted using a reaction-diffusion model.

DISCUSSION

In this study, we show that the accurate estimation of the diffusion rate of a fluorescently labeled complex in the cell by FRAP must take into account the binding affinity of the fluorescent tag to the substrate.

By exploring extensively the reaction parameter space, we studied the possible FRAP behaviors in the case of two interacting mobile species. We found that only in a small subset of points are the full reaction-diffusion equations required to fit FRAP data, and that for the majority of the cases, simple diffusion models yield good fits. However, extraction of binding information from fits should be done cautiously, as experiments performed in a pseudoeffective diffusion regime could be confused with proper effective diffusion behavior and lead to erroneous conclusions. In the effective diffusion regime, we show that, provided the diffusion coefficients of the free molecules and the complex are known, it is possible to accurately determine the percentage of fluorescent proteins bound to the substrate.

We have previously reasoned that if practically all nuclear mRNAs contain a poly(A) tail that is specifically covered by the PABPN1 protein, a fusion of PABPN1 to GFP could be used to analyze the dynamics of mRNPs in the nucleus (18). Because biochemical data and fluorescence loss in photobleaching experiments indicated that most (>95%) of the GFP-PABPN1 molecules expressed in cells were actually bound to poly(A)RNA (32), we considered that the complexes formed by GFP-PABPN1 and poly(A)RNA represented a single population. Accordingly, we used a simple single-component effective diffusion model to fit the experimental FRAP data, and we calculated a diffusion coefficient of 0.6 $\mu m^2\ s^{-1}$. In this study, we show that the same experimental FRAP recovery curves can be equally fitted with an alternative model that considers the binding of GFP-PABPN1 to poly(A)-RNA as a reversible and not very tight process. The model assumes that, although at any given moment most GFP-PABPN1 molecules are bound to RNA, there is a constant exchange between bound and nonbound GFP pools. Free molecules were considered to diffuse at 25 $\mu m^2\ s^{-1}$, according to their molecular weight, whereas the complexes were assumed to move at 0.04 $\mu m^2\ s^{-1}$ (29). The results show that the effective diffusion coefficient measured by FRAP is much higher than the mobility of the mRNP complex, because fluorescent molecules not bound to RNA diffuse at rates ~500-fold faster than bound molecules.

A recent study has elegantly avoided the problem of measuring the mobility of nonbound fluorescent probes through the use of molecular beacons that only fluoresce when hybridized to the specific target RNA substrate (31). Using this approach, mRNPs were found to diffuse at an average rate of 0.033 $\mu m^2/s$ (31). A very similar value (0.04 $\mu m^2\ s^{-1}$) was reported for the diffusion of an mRNA tagged with multiple GFP-MS2 molecules, and measured by single-particle tracking (29,30). In this case, where the movement

of a cluster of GFP-MS2 molecules is directly tracked, the reversible binding of the fluorescent tag to the mRNP is not a problem, because only fluorescent mRNPs are detected as single particles, whereas single, unbound GFP-MS2 molecules are not.

Theoretical approaches and computational simulations have been used to predict the time that an mRNA takes to reach a pore (32,42). Assuming that mRNPs move according to a three-dimensional Pearson-type random walk inside a spherical nucleus of 8-μm radius; that the mRNP particles do not interact with each other and cannot enter inside the volume occupied by nucleoli; and that the nucleus contains 2000 randomly scattered pores at the surface, each pore with a functional diameter of ~40 nm (43), then the time an average mRNP particle takes to move from a random position in the nucleus to a nuclear pore by Brownian motion is ~6.1 min for $D = 0.033\ \mu m^2\ s^{-1}$ and ~20 s for $D = 0.6\ \mu m^2\ s^{-1}$ (32). Taking into account the results of classical pulse-chase experiments indicating that radioactively labeled mRNAs were detected in the cytoplasm ~5–10 min after synthesis (44), we consider that a value within the range 0.02–0.04 $\mu m^2\ s^{-1}$ most likely reflects an accurate estimate of the diffusion rate of an average mRNP in the nucleus.

The authors are grateful to Tom Misteli (National Institutes of Health/National Cancer Institute, Bethesda, MD) for advice, and José Rino (Institute of Molecular Medicine, University of Lisbon, Lisbon, Portugal) for helpful comments and critical reading of the manuscript.

This work was supported by Fundação para a Ciência e a Tecnologia (Portugal) and the European Commission (LSHG-CT-2003-503259).

REFERENCES

1. Mendes Soares, L. M., and J. Valcarcel. 2006. The expanding transcriptome: the genome as the 'Book of Sand'. *EMBO J.* 25:923–931.
2. Shav-Tal, Y., R. H. Singer, and X. Darzacq. 2004. Imaging gene expression in single living cells. *Nat. Rev. Mol. Cell Biol.* 5:855–861.
3. Misteli, T. 2001. Protein dynamics: implications for nuclear architecture and gene expression. *Science.* 291:843–847.
4. Lippincott-Schwartz, J., N. Altan-Bonnet, and G. H. Patterson. 2003. Photobleaching and photoactivation: following protein dynamics in living cells. *Nat. Cell Biol. Suppl.*:S7–S14.
5. Phair, R. D., and T. Misteli. 2001. Kinetic modelling approaches to in vivo imaging. *Nat. Rev. Mol. Cell Biol.* 2:898–907.
6. Sprague, B. L., and J. G. McNally. 2005. FRAP analysis of binding: proper and fitting. *Trends Cell Biol.* 15:84–91.
7. Desterro, J. M., L. P. Keegan, M. Lafarga, M. T. Berciano, M. O'Connell, and M. Carmo-Fonseca. 2003. Dynamic association of RNA-editing enzymes with the nucleolus. *J. Cell Sci.* 116:1805–1818.
8. Tavanez, J. P., P. Calado, J. Braga, M. Lafarga, and M. Carmo-Fonseca. 2005. In vivo aggregation properties of the nuclear poly(A)-binding protein PABPN1. *RNA.* 11:752–762.
9. Boisvert, F. M., M. J. Kruhlak, A. K. Box, M. J. Hendzel, and D. P. Bazett-Jones. 2001. The transcription coactivator CBP is a dynamic component of the promyelocytic leukemia nuclear body. *J. Cell Biol.* 152:1099–1106.
10. Trinkle-Mulcahy, L., J. E. Sleeman, and A. I. Lamond. 2001. Dynamic targeting of protein phosphatase 1 within the nuclei of living mammalian cells. *J. Cell Sci.* 114:4219–4228.
11. McNally, J. G., W. G. Muller, D. Walker, R. Wolford, and G. L. Hager. 2000. The glucocorticoid receptor: rapid exchange with regulatory sites in living cells. *Science.* 287:1262–1265.
12. Harrer, M., H. Luhrs, M. Bustin, U. Scheer, and R. Hock. 2004. Dynamic interaction of HMGA1a proteins with chromatin. *J. Cell Sci.* 117:3459–3471.
13. Lam, M. H., R. J. Thomas, K. L. Loveland, S. Schilders, M. Gu, T. J. Martin, M. T. Gillespie, and D. A. Jans. 2002. Nuclear transport of parathyroid hormone (PTH)-related protein is dependent on microtubules. *Mol. Endocrinol.* 16:390–401.
14. Lang, I., M. Scholz, and R. Peters. 1986. Molecular mobility and nucleocytoplasmic flux in hepatoma cells. *J. Cell Biol.* 102:1183–1190.
15. Handwerger, K. E., C. Murphy, and J. G. Gall. 2003. Steady-state dynamics of Cajal body components in the *Xenopus* germinal vesicle. *J. Cell Biol.* 160:495–504.
16. Sprague, B. L., R. L. Pego, D. A. Stavreva, and J. G. McNally. 2004. Analysis of binding reactions by fluorescence recovery after photobleaching. *Biophys. J.* 86:3473–3495.
17. Kimura, H., K. Sugaya, and P. R. Cook. 2002. The transcription cycle of RNA polymerase II in living cells. *J. Cell Biol.* 159:777–782.
18. Calapez, A., H. M. Pereira, A. Calado, J. Braga, J. Rino, C. Carvalho, J. P. Tavanez, E. Wahle, A. C. Rosa, and M. Carmo-Fonseca. 2002. The intranuclear mobility of messenger RNA binding proteins is ATP dependent and temperature sensitive. *J. Cell Biol.* 159:795–805.
19. Beaudouin, J., F. Mora-Bermudez, T. Klee, N. Daigle, and J. Ellenberg. 2006. Dissecting the contribution of diffusion and interactions to the mobility of nuclear proteins. *Biophys. J.* 90:1878–1894.
20. Sprague, B. L., F. Muller, R. L. Pego, P. M. Bungay, D. A. Stavreva, and J. G. McNally. 2006. Analysis of binding at a single spatially localized cluster of binding sites by fluorescence recovery after photobleaching. *Biophys. J.* 91:1169–1191.
21. Kubitscheck, U., P. Wedekind, and R. Peters. 1998. Three-dimensional diffusion measurements by scanning microphotolysis. *J. Microsc.* 192: 126–138.
22. Braga, J., J. M. Desterro, and M. Carmo-Fonseca. 2004. Intracellular macromolecular mobility measured by fluorescence recovery after photobleaching with confocal laser scanning microscopes. *Mol. Biol. Cell.* 15:4749–4760.
23. Wei, X., V. G. Henke, C. Strubing, E. B. Brown, and D. E. Clapham. 2003. Real-time imaging of nuclear permeation by EGFP in single intact cells. *Biophys. J.* 84:1317–1327.
24. Shimi, T., T. Koujin, M. Segura-Totten, K. L. Wilson, T. Haraguchi, and Y. Hiraoka. 2004. Dynamic interaction between BAF and emerin revealed by FRAP, FLIP, and FRET analyses in living HeLa cells. *J. Struct. Biol.* 147:31–41.
25. Phair, R. D., and T. Misteli. 2000. High mobility of proteins in the mammalian cell nucleus. *Nature.* 404:604–609.
26. Politz, J. C., E. S. Browne, D. E. Wolf, and T. Pederson. 1998. Intranuclear diffusion and hybridization state of oligonucleotides measured by fluorescence correlation spectroscopy in living cells. *Proc. Natl. Acad. Sci. USA.* 95:6043–6048.
27. Politz, J. C., R. A. Tuft, T. Pederson, and R. H. Singer. 1999. Movement of nuclear poly(A) RNA throughout the interchromatin space in living cells. *Curr. Biol.* 9:285–291.
28. Snaar, S. P., P. Verdijk, H. J. Tanke, and R. W. Dirks. 2002. Kinetics of HCMV immediate early mRNA expression in stably transfected fibroblasts. *J. Cell Sci.* 115:321–328.
29. Shav-Tal, Y., X. Darzacq, S. M. Shenoy, D. Fusco, S. M. Janicki, D. L. Spector, and R. H. Singer. 2004. Dynamics of single mRNPs in nuclei of living cells. *Science.* 304:1797–1800.
30. Molenaar, C., A. Abdulle, A. Gena, H. J. Tanke, and R. W. Dirks. 2004. Poly(A)+ RNAs roam the cell nucleus and pass through speckle domains in transcriptionally active and inactive cells. *J. Cell Biol.* 165:191–202.
31. Vargas, D. Y., A. Raj, S. A. Marras, F. R. Kramer, and S. Tyagi. 2005. Mechanism of mRNA transport in the nucleus. *Proc. Natl. Acad. Sci. USA.* 102:17008–17013.

32. Braga, J., J. Rino, and M. Carmo-Fonseca. 2004. Photobleaching microscopy reveals the dynamics of mRNA-binding proteins inside live cell nuclei. *Prog. Mol. Subcell. Biol.* 35:119–134.

33. Braeckmans, K., B. G. Stubbe, K. Remaut, J. Demeester, and S. C. De Smedt. 2006. Anomalous photobleaching in fluorescence recovery after photobleaching measurements due to excitation saturation–a case study for fluorescein. *J. Biomed. Opt.* 11:044013.

34. Peters, R., and U. Kubitscheck. 1999. Scanning microphotolysis: three-dimensional diffusion measurement and optical single-transporter recording. *Methods.* 18:508–517.

35. Hinow, P., C. E. Rogers, C. E. Barbieri, J. A. Pietenpol, A. K. Kenworthy, and E. Dibenedetto. 2006. The DNA binding activity of p53 displays reaction-diffusion kinetics. *Biophys. J.* 91:330–342.

36. Lele, T. P., and D. E. Ingber. 2005. A mathematical model to determine molecular kinetic rate constants under non-steady state conditions using fluorescence recovery after photobleaching (FRAP). *Biophys. Chem.* 120:32–35.

37. Sadegh Zadeh, K., H. J. Montas, and A. Shirmohammadi. 2006. Identification of biomolecule mass transport and binding rate parameters in living cells by inverse modeling. *Theor. Biol. Med. Model.* 3:36.

38. Crank, J. 1975. The Mathematics of Diffusion. Clarendon Press, Oxford, UK.

39. Axelrod, D., D. E. Koppel, J. Schlessinger, E. Elson, and W. W. Webb. 1976. Mobility measurement by analysis of fluorescence photobleaching recovery kinetics. *Biophys. J.* 16:1055–1069.

40. Wahle, E., A. Lustig, P. Jeno, and P. Maurer. 1993. Mammalian poly(A)-binding protein II. Physical properties and binding to polynucleotides. *J. Biol. Chem.* 268:2937–2945.

41. Johansson, H. E., D. Dertinger, K. A. LeCuyer, L. S. Behlen, C. H. Greef, and O. C. Uhlenbeck. 1998. A thermodynamic analysis of the sequence-specific binding of RNA by bacteriophage MS2 coat protein. *Proc. Natl. Acad. Sci. USA.* 95:9244–9249.

42. Kuthan, H. 2005. Temporal fluctuation of nuclear pore complex localization by single diffusing mRNP complexes. *J. Theor. Biol.* 236:256–262.

43. Ribbeck, K., and D. Gorlich. 2001. Kinetic analysis of translocation through nuclear pore complexes. *EMBO J.* 20:1320–1330.

44. Lewin, B. 1980. Gene Expression. Eucaryotic Chromosomes. John Wiley & Sons, New York.